Knölker Iron Catalysts for Hydrogenation Revisited: A Nonspectator Solvent and Fine-Tuning

Martí Gimferrer, Nicolas Joly, Sílvia Escayola, Eduard Viñas, Sylvain Gaillard, Miquel Solà, Jean-Luc Renaud, Pedro Salvador, Albert Poater

ORGANOMETALLICS

pubs.acs.org/Organometallics Article

Knölker Iron Catalysts for Hydrogenation Revisited: A Nonspectator Solvent and Fine-Tuning

Martí Gimferrer, Nicolas Joly, Sílvia Escayola, Eduard Viñas, Sylvain Gaillard, Miquel Solà, Jean-Luc Renaud,* Pedro Salvador,* and Albert Poater*

Cite This: *Organometallics* 2022, 41, 1204–1215 Read Online

ACCESS | Metrics & More | Article Recommendations | Supporting Information

ABSTRACT: The reductive amination process under hydrogen at high pressure catalyzed by iron complexes is of great synthetic interest. In this work, we report density functional theory (DFT) studies on the reductive amination catalyzed by a Knölker-type iron complex. Different modifications of the catalyst are explored to improve the efficiency and guide experiments toward milder conditions. DFT calculations in conjunction with analysis of the chemical structure in terms of geometry, fragment partial charges, effective oxidation states (EOS), and aromaticity allows us to conclude that the presence of electron-withdrawing substituents on the cyclopentadienone ring induces a decrease of the activation barriers of most relevant steps, leading to a more efficient catalysis. The present work is a clear example that predictive catalysis can have a fundamental role in sustainable catalytic transformations.

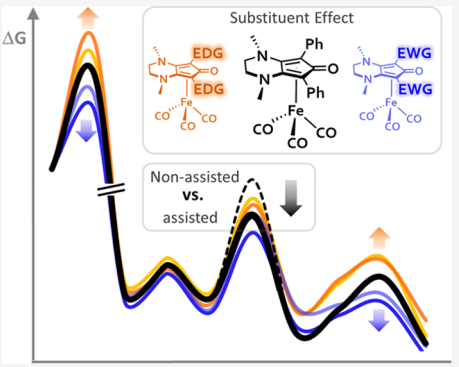

INTRODUCTION

Hydrogenation reactions of double bonds,[1] either C=C[2] or C=O[3] bonds, are extensively used to synthesize compounds for the pharmaceutical industry[4] and the agricultural sector. However, when it comes to C=N bonds, hydrogenation is still a challenge for homogeneous catalysis.[5] Noble metals such as rhodium, palladium, ruthenium, or iridium were initially reported for the reductive amination of carbonyl compounds, using molecular hydrogen,[6] formic acid,[7] transfer hydrogenation,[8] or borrowing hydrogen.[9,10] Among all catalysts discovered, ruthenium became the most extensively used metal.[11] In particular, Noyori[12] and Shvo[13] catalysts (represented in Scheme 1) have been used for the hydrogenation of the previously mentioned polar functional groups.[14]

Later, following the increasing trend of replacing noble metals with earth-abundant and sustainable first-row transition metals, Casey et al.[15] proposed the use of a Knölker-type catalyst for the reduction of carbonyl substrates. The Knölker complex[16] is an iron analogue of Shvo catalyst, and it presents bifunctional nature since it has both proton- and hydride-donating sites on the hydroxyl ligand and the metal center, respectively.

Despite the major advantages offered by the use of first-row transition metals, in terms of abundance and ecofriendly properties, such substitution is required but also is one of the main challenges of modern organometallic chemistry due to the different electronic and chemical properties that these owe.[17] Certainly, research on iron-based catalysts is promising,[18] and for this reason, the understanding of the reductive amination under hydrogen at high pressure catalyzed by iron complexes is of great interest.[19] First, Bhanage et al. reported the reductive amination under harsh conditions (high temperatures and hydrogen pressure) using $FeSO_4$ with ethylenediaminetetraacetic acid (EDTA).[6e] Then, Beller et al. showed that iron−carbonyl complexes can be activated in reductive amination by carbonyl compounds with aromatic amines.[2] From these, Renaud, among other researchers, determined that the Knölker catalyst, together with its modifications,[20−22] catalyzes the reductive amination of aliphatic carbonyl compounds, like ketones or aldehydes,[23] as well as CO_2,[24] using molecular hydrogen as a reducing agent (see Scheme 2). In particular, catalysts afforded complete

Scheme 1. Noyori (a) and Shvo (b) Catalysts

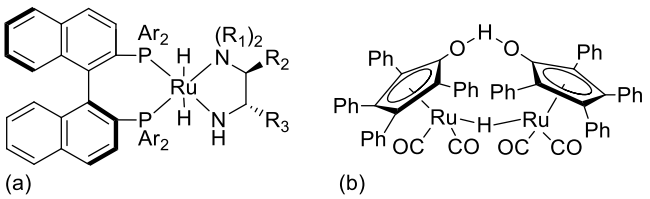

Received: February 24, 2022
Published: May 6, 2022

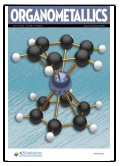

https://doi.org/10.1021/acs.organomet.2c00099
Organometallics 2022, 41, 1204−1215

Scheme 2. General Scheme of C═N Bond Hydrogenation

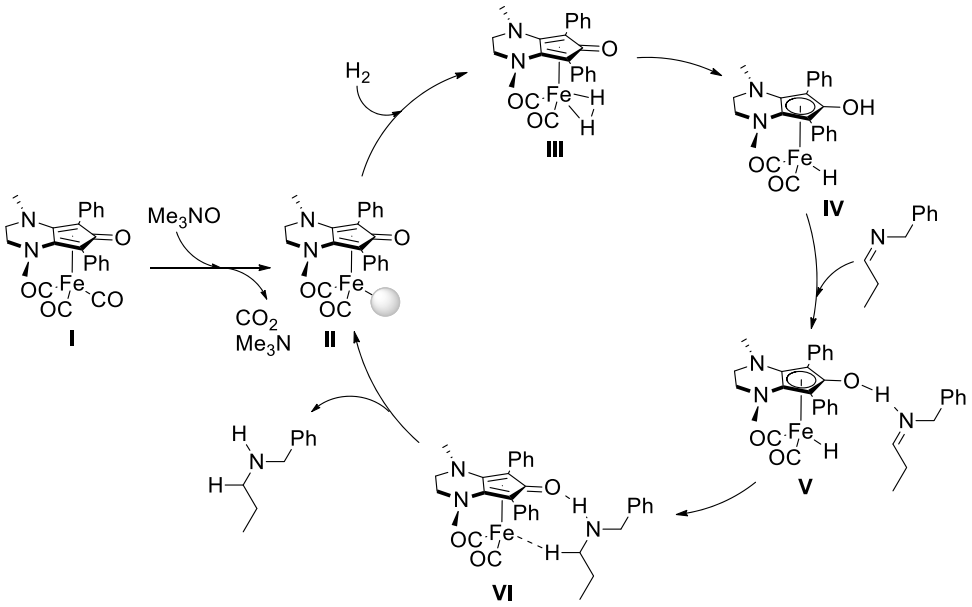

reductive amination at 44 °C, moving toward milder conditions.[22]

Beller's studies[23a,d] in combination with the following work of Poater and Renaud[25] demonstrated that modifying the nature of the substituents on the Knölker-type iron tricarbonyl cyclopentadienone complex shown in Scheme 3 not only improves the reactivity and chemoselectivity but also allows the reduction of unsaturated aldehydes together with its reductive amination. Nevertheless, such modifications have to be done carefully since subtle changes in the catalyst can also reduce its activity.[26]

To increase the Lewis base character of these complexes, the *N,N′*-dimethyl-3,4-ethylendiamino-substituted cyclopentadienone was synthesized to act as a ligand, obtaining complex **1**. Experimental results obtained and supported by DFT calculations indicate that catalyst **1** presents better yields for the reaction than complexes **2** and **3**.[22] In addition, the phenyl groups on the five-membered ring avoid the undesired formation of stable dimers, enhancing the catalytic efficiency.

A systematic study modifying Knölker-type system **1** is required to improve its catalytic activity, and consequently the reaction conditions for the reductive amination. For this reason, we present a computational study throughout DFT calculations for the whole reaction pathway of C═N bond hydrogenation, *i.e.*, the reductive amination,[27] with modifications of catalyst **1**. In line with similar recent strategies,[28] the aim of this study is to substitute the phenyl groups of the cyclopentadienone ligand with alternative moieties that bear different electronic properties, thus moving toward predictive catalysis.

RESULTS AND DISCUSSION

The complete mechanistic cycle of reductive amination using iron complex **1** was first described in 2015 by means of density functional theory (DFT) calculations.[22] Here, we re-evaluate it in Figure 1 at the M06/cc-pVTZ—SDD(pcm-EtOH)//BP86/SVP—SDD level of theory (see Computational Details) to be used as a reference when modifying the substituents of cyclopentadienone (see Scheme 3). The imine substrate originates from the condensation of reactants of Scheme 3c,

Scheme 3. Cyclopentadienone Iron Tricarbonyl Complex: (a) Transition Metal-Type Frustrated Lewis Pair, (b) Iron Knölker Derivative Catalysts Introduced by Renaud et al.,[21] (c) Reductive Amination Using Catalysts 1−3, and (d) Catalyst Studied Here, Replacing the R_1 Substituent

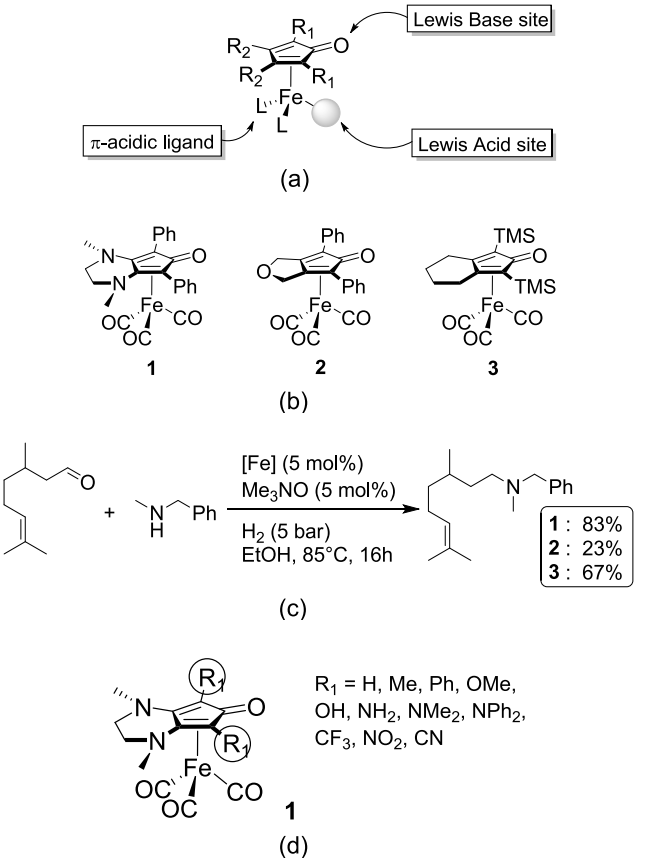

where the long aliphatic chain of the amine is replaced by an ethyl group in the computational model. First, species **I** is activated when releasing one CO ligand *via* reductive

https://doi.org/10.1021/acs.organomet.2c00099
Organometallics 2022, 41, 1204−1215

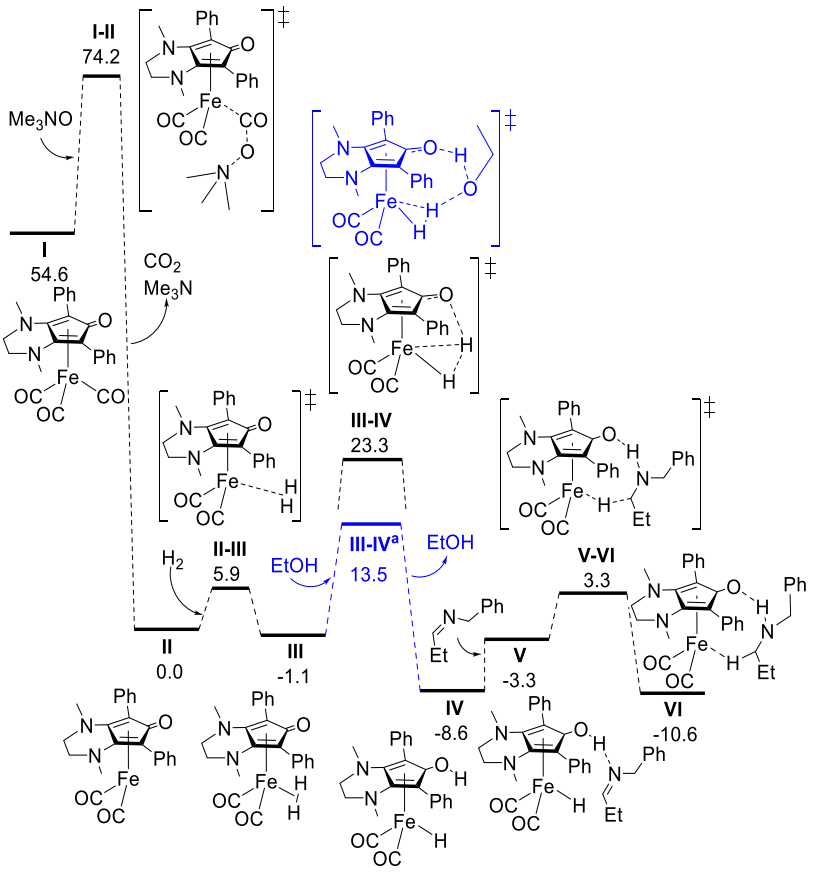

Figure 1. Catalytic cycle of reductive amination using complex **1** (relative Gibbs energies with respect to the catalytic active species **II** in kcal/mol at the M06/cc-pVTZ—SDD(pcm-EtOH)//BP86/SVP—SDD level of theory; a = proton transfer assisted by one ethanol molecule.

elimination with trimethylamine-*N*-oxide (Me_3NO), forming the 16 electron species **II** with an energy cost of 19.6 kcal/mol (**I**–**II**) (see Figure 2a). This stoichiometric process corresponds to the activation of the catalysts and accounts for its induction period. Being an energetically demanding step, it deserves proper attention, but still, species **II** is considered the catalytic active species. Then, the catalytic cycle proceeds as follows. Electron-deficient intermediate **II** reacts with molecular hydrogen through a low kinetically demanding transition state (TS) **II**–**III** with an energy cost of 5.9 kcal/mol. Formed intermediate **III** has the H_2 π-coordinated to the metallic center. Subsequently, **III** forms iron hydride **IV** with a significant energy barrier through TS **III**–**IV** (24.4 kcal/mol), as suggested in 2010 by Berkessel and Chen for the Knölker catalysts **2**[29] and **3**[30] (Scheme 3b). In this particular step, one hydrogen atom is transferred from the π-coordinated H_2 to the C═O (keto) group of the cyclopentadienone, forming a hydroxyl group that can play the role of a Brönsted acid. In the presence of an imine, such as in intermediate **V**, hydrogenation takes place to form the corresponding secondary amine, still bonded to the catalyst as in intermediate **VI**, with an energy penalty of 11.9 kcal/mol from **IV**. Releasing the amine formed regenerates intermediate **II**, closing the catalytic cycle.

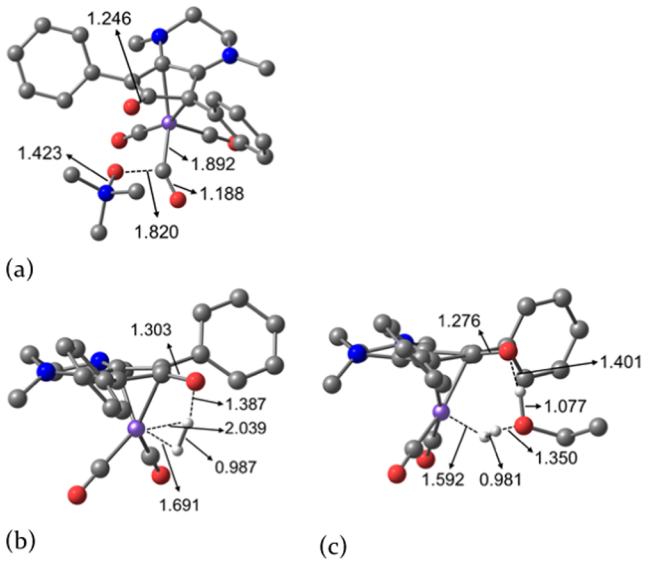

Figure 2. Transition states (a) **I**–**II**, (b) nonassisted **III**–**IV**, and (c) ethanol-assisted **III**–**IV**. Selected distances are shown in Å. Non-relevant H-atoms are omitted for clarity.

The energetics of the reaction pathway is very similar to those reported in ref 22. Previously, the H_2 activation in the **III** → **IV** step was found to be the rate-determining step (rds) of the reaction.[22] However, in agreement with previous studies from Chen and co-workers,[30] we found that this step can be assisted by an explicit solvent molecule (either alcohol or water), lowering its energy cost.[31] Thus, the **III** → **IV** step requires 14.7 or 17.2 kcal/mol when assisted by one ethanol or one water molecule, respectively, meaning that the initial preactivation of the catalyst involving CO release is even more kinetically demanding than the rds of the catalytic pathway.

https://doi.org/10.1021/acs.organomet.2c00099
Organometallics 2022, 41, 1204−1215

Table 1. Relative Gibbs Energies (with Respect to the Catalytic Active Species II) Obtained at the M06/cc-pVTZ—SDD(pcm-EtOH)//BP86/SVP—SDD Level of Theory (in kcal/mol) for the Differently Substituted Catalysts 1[a]

	H	Me	Ph	OMe	OH	NH_2	NMe_2	NPh_2	CF_3	NO_2	average	standard deviation
I	55.5	54.2	54.6	51.3	52.9	52.2	53.0	53.6	53.9	56.2	53.8	1.5
I–II	77.2	74.9	74.2	74.8	76.1	75.3	80.0	74.6	69.1	68.4	74.5	3.5
II	0.0	0.0	0.0	0.0	0.0	0.0	0.0	0.0	0.0	0.0	0.0	0.0
II–III	5.8	5.6	5.9	4.4	4.7	5.0	3.6	2.8	5.1	5.8	4.9	1.0
III	−2.1	−2.5	−1.1	−5.0	−3.1	−2.3	−3.7	−4.0	−4.2	−2.4	−3.0	1.2
III–IV	24.9	24.2	23.3	25.6	28.8	24.7	25.5	27.9	28.2	29.5	26.2	2.2
III–IV[a]	15.5	15.1	13.5	14.9	17.0	16.7	16.9	18.0	14.3	12.3	15.4	1.7
III–IV[b]	17.1	16.3	16.1	15.7	19.7	17.5	17.1	17.3	15.8	14.4	16.7	1.4
IV	−5.1	−6.7	−8.6	−3.6	−2.7	−5.9	−5.4	−4.7	−3.8	−5.5	−5.2	1.7
V	−2.5	−3.6	−3.3	−1.7	−1.1	−0.1	1.5	1.0	−3.1	−2.9	−1.6	1.8
V–VI	5.6	3.4	3.3	4.4	4.5	5.2	5.3	3.4	−0.9	−0.3	3.4	2.3
VI	−11.2	−11.7	−10.6	−10.5	−12.4	−11.3	−7.3	−8.1	−11.9	−11.7	−10.7	1.7
ΔG (I–II)	21.7	20.7	19.6	23.5	23.2	23.1	27.0	21.0	15.2	12.2	20.7	4.3
ΔG (III–IV)	26.9	26.8	24.4	30.5	31.9	26.9	29.2	31.8	32.4	32.0	29.3	2.8
ΔG (III–IV[a])	17.5	17.7	14.7	19.8	20.1	18.9	20.6	21.9	18.5	14.8	18.4	2.4

[a]Me = methyl, Ph = phenyl. a, b = proton transfer assisted by one ethanol and one water molecule, respectively.

Scheme 4. Most Relevant Resonance Structures for Cyclopentadienone

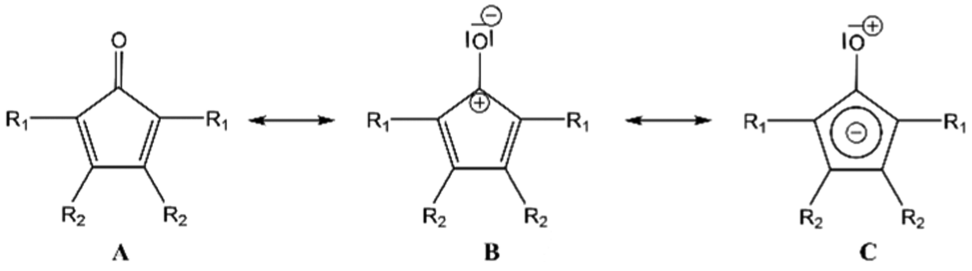

The optimized geometries of the nonassisted and ethanol-assisted TS **III–IV** are depicted in Figure 2b,c. A plausible explanation for the decrease in the energy of the TS is the reduction of the strain when moving from a five-membered (nonassisted) to a seven-membered (assisted) ring, formed by the metal, C═O (keto), hydrogen, and the −OH of the solvent in the assisted TS.[10g] A similar effect on the **III–IV** barrier is also found for catalyst **3**. When assisted by an ethanol molecule, a barrier of 16.9 kcal/mol is obtained, *ca.* 2 kcal/mol higher in energy than for catalyst **1**. This is in agreement with the reported experimental evidence.[22]

Let us focus our attention on some additional aspects of the mechanism. First, the last step, *i.e.*, **V** → **VI**, where the C═N bond of the *N*-benzyl-1-propanimine is hydrogenated, was faced as a step-wise process,[29,32,33] but for these kind of substrates, this alternative way with two sequential H-transfers is not feasible. Second, the hydrogenated product could be reconciled to the vacant position of Fe before closing the cycle but not by making a H-bridge as in intermediate **VI** (which is the structure readily formed from TS **V–VI**, as IRC calculations confirm) but coordinated through the nitrogen atom.[15b] Such intermediate **VI'** is stabilized with respect to **VI** by 13.6 kcal/mol. Similarly, as pointed out by one of the reviewers, a solvent molecule like EtOH could coordinate to the vacant position of Fe on the **II** species, thus blocking the reaction. As could be anticipated, since the coordination of alcohols is less favored than amines, its formation is *ca.* 10.6 kcal/mol less stable than the above-mentioned intermediate **VI'** (*i.e.*, the coordination of the hydrogenation product) for the H-substituted catalyst.

The imine-iminium/enamine equilibrium was also considered from intermediate **V**. Although the barrier for this pathway was already found[22] to be over 23.0 kcal/mol more demanding in the case of the enamine, we revaluate it here to take into account the effect of explicit solvent molecules assisting the process. With either EtOH or water, the enamine pathway is further destabilized by 20.0 and 18.6 kcal/mol, respectively.

The main focus of this work is to assess the substituent effect in the reaction pathway by replacing both phenyl groups on the cyclopentadienone ligand with a series of other electron-donating (EDG) and electron-withdrawing (EWG) ligands, including H, CH_3, CF_3, NO_2, OMe, OH, NMe_2, NPh_2, and NH_2 (Me = methyl and Ph = phenyl). The resulting relative Gibbs energies (ΔG_F) along the catalytic cycle are compiled in Table 1. The most noticeable effect is a significant lowering of the barrier for the catalyst activation **I–II** step with $R_1 = CF_3$ and $R_1 = NO_2$ substitution as compared to any other substituent. In particular, the energy barrier for the original phenyl-substituted complex **1** amounts to 19.6 kcal/mol, while the barrier decreases to 15.2 and 12.2 kcal/mol with $R_1 = CF_3$ and $R_1 = NO_2$ substitution, respectively. Scheme 4 shows that the electronic structure of cyclopentadienone can be described mainly by resonance structure **A** with a certain influence of structures **B** and **C**. The presence of an EWG in R_1 could increase the weight of structure **C**, leading to an enhanced donation from the cyclopentadienone to the metal, which in turn could make the CO ligand more labile. These intricate electronic aspects will be analyzed in detail (*vide infra*). Conversely, substitution by EDG such as $R_1 = OR$ or $R_1 = NR_2$

https://doi.org/10.1021/acs.organomet.2c00099
Organometallics 2022, 41, 1204−1215

Table 2. NICS(1)$_{out}$ Evaluated at the BP86/6-31+G**//BP86/SVP—SDD Level for 5-MR of Cyclopentadienone (Cp) and the Differently Substituted Intermediates I–IV[a]

	H	CH_3	Ph	OMe	OH	NH_2	NMe_2	NPh_2	CF_3	NO_2
Cp^{2-}	−2.4	−2.0	−1.7	−5.6	−2.4	−5.4	−5.2	−2.7	−3.2	−2.5
Cp	2.0	1.6	2.2	5.3	6.6	3.6	1.8	2.7	−0.2	−0.2
I	−9.7	−10.6	−8.9	−10.5	−11.0	−10.6	−10.6	−8.6	−9.5	−9.0
II	−7.5	−7.7	−6.5	−7.6	−8.5	−8.1	−7.1	−6.7	−7.9	−7.8
III	−10.0	−11.1	−9.1	−11.3	−11.7	−11.4	−10.6	−8.6	−10.0	−9.4
IV	−11.5	−11.8	−10.4	−12.3	−12.8	−12.4	−12.3	−10.7	−11.5	−10.7

[a]Me = methyl, Ph = phenyl.

Table 3. Topological Fuzzy Voronoi Cell (TFVC) Partial Charges of the Fe Center (Top), and the Cyclopentadienone Ligand (Bottom) at the M06/cc-pVTZ—SDD(pcm-EtOH)//BP86/SVP—SDD Level for Intermediates I–IV[a]

	H	CH_3	Ph	OMe	OH	NH_2	NMe_2	NPh_2	CF_3	NO_2
I	0.838	0.817	0.822	0.793	0.774	0.782	0.829	0.854	0.860	0.868
II	0.786	0.778	0.783	0.746	0.747	0.755	0.773	0.791	0.820	0.836
III	0.843	0.828	0.842	0.804	0.787	0.805	0.842	0.852	0.863	0.877
IV	0.809	0.809	0.826	0.781	0.773	0.790	0.803	0.836	0.826	0.842
I	−0.213	−0.175	−0.183	−0.099	−0.111	−0.067	−0.207	−0.258	−0.353	−0.399
II	−0.222	−0.192	−0.241	−0.170	−0.177	−0.160	−0.198	−0.265	−0.346	−0.388
III	−0.252	−0.214	−0.231	−0.179	−0.146	−0.146	−0.232	−0.274	−0.374	−0.398
IV	0.010	−0.002	−0.044	0.036	0.028	0.072	0.006	−0.081	−0.156	−0.219

[a]Me = methyl, Ph = phenyl.

leads to an increase in the activation barrier as compared to the original **1** species. The highest energy barrier (27.2 kcal/mol) is found for the electron-donating NMe_2 substituent. Close inspection of the TS structure reveals a significant number of $CH_3\cdots CH_3$ close contacts that destabilize the structure as compared to that of other electronically similar substituents. On the other hand, the unexpectedly low barrier of 21.0 kcal/mol for the **I**–**II** step and $R_1 = NPh_2$ is surprising, bearing in mind that the barrier for $R_1 = NMe_2$ is 27.0 kcal/mol. Inspection of the reaction coordinate clearly shows the concerted motion of the phenyl rings, guided by noncovalent interactions with the amine oxide moiety.

The substituent effect is smaller in the steps of the catalytic cycle but still noticeable and apparently unrelated to either their electron-donating/withdrawing or steric features (see standard deviation (std) values in Table 1).

One interesting observation is that the planarity of the cyclopentadienone ligand keeps changing along the reaction pathway, as shown in Table S26 of the supporting material. The ligand is planar when isolated, but upon coordination with the metal center in **1**, the C═O group notably deviates from planarity, thus affording a η^4 coordination. Such a deviation is kept in the **I**–**II** transition state structure, but the ligand regains planarity upon the formation of the electron-deficient structure **II**. Then, the ligand loses planarity again when H_2 is coordinated to the Fe center in structure **III**. In the key steps **III**–**IV**, in the absence of assisting EtOH or H_2O molecules, the transition state structure presents the planar form of the ligand in the formation of the aforementioned four-membered ring. On the contrary, when assisted by an EtOH or H_2O molecule, the ligand loses somewhat its planarity in the five-membered ring transition state structure. When the proton is transferred to the C═O group in **IV**, the ligand regains the planarity, which is kept until structure **VI** is formed, prior to the release of the amine.

These observations suggest an aromatization/dearomatization of the cyclopentadienone ligand, which might play a relevant role in the catalytic cycle and in the electronic effects of the ligand substitution. To test this hypothesis, we have computed the NICS values at the center of the five-membered ring and at a 1 Å distance above it. The results obtained are given in Table S11 and Table 2, respectively. Remarkably, the planar isolated cyclopentadienone exhibits small positive values of NICS, so it is in fact nonaromatic,[34] in line with the analysis of Pal et al.[35] Upon coordination with the metal to form **I**, the ligand loses its planarity but, conversely, exhibits an aromatic character. All NICS values are around −10 ppm on average, similar to that of benzene (−9.9 ppm at the current level of theory),[36] and they are rather independent of the nature of the substituent. Also, the C–C distances along the ring tend to equalize as compared to those of the free ligand.

For the electron-deficient structure **II**, the NICS values still indicate an aromatic character, but the numbers (in absolute value) are smaller than those of **I**, despite the ligand being essentially planar. Turning to structure **III**, the ligand loses planarity again, recovering the aromatic values similar to those of structure **I**. Again, no clear trend can be derived from the ligand substitution. Finally, upon protonation of the C═O moiety, the ligand becomes planar and the NICS value becomes even more negative, more in line with the value of the free anionic ligand (−9.2 ppm for **1**). At this point, it becomes apparent that the aromaticity of the ring is neither connected with the deviation of planarity nor with the substituent effect (at least as far as the NICS index is concerned). Moreover, it cannot explain the rather significant substituent effect observed on the energies of the first step of the reaction.

As shown in Table 2, the (planar) dianionic free ligand (Cp^{2-}) is slightly aromatic according to the NICS values. Indeed, the highest-occupied molecular orbital (HOMO) (lowest-unoccupied molecular orbital (LUMO) of the neutral ligand) is a π^* orbital of the ring so that in the dianionic case, the five-membered ring accommodates 6π electrons.

The aromatic character of the ligand upon coordination (being nonplanar or planar) can be explained in terms of

https://doi.org/10.1021/acs.organomet.2c00099
Organometallics 2022, 41, 1204–1215

electron transfer from the metal center to the π-type LUMO of the ligand. But since the overall charge of the ligand in the complex is rather close to zero (see Table 3), there must be an additional channel for ligand donation to the metal. In this sense, the effective fragment orbitals (EFOs)[37] are very useful for both visualization and quantification of this electron flow within a complex without recurring additional reference fragment calculations. They also afford the assignation of formal oxidation states (OS) by means of the so-called effective oxidation state (EOS) analysis.[38,39] The EFOs are obtained from the molecular density for each molecular fragment, and typically resemble the MOs of the free fragment. The embedding effect of the fragment within the molecule induces some polarization/distortion of the EFOs, as compared to the free MOs, but most importantly, the EFOs exhibit fractional occupations.

The relevant EFOs that explain the electron flow between the cyclopentadienone ligand and the metal are depicted in Figure 3. The two π-type EFOs on the ligand (Figure 3a,b) can

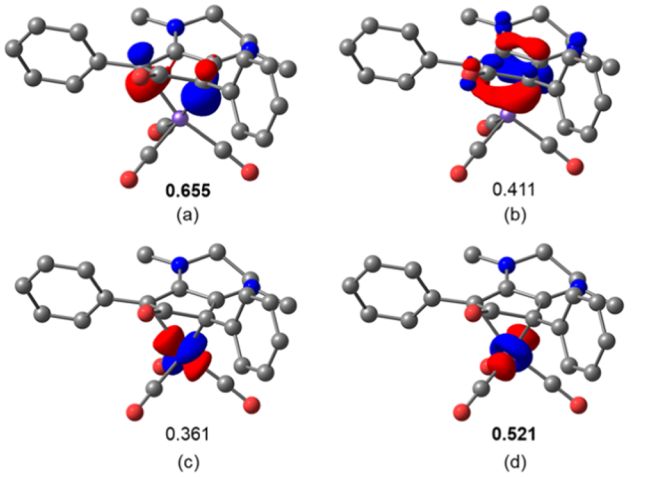

Figure 3. Effective fragment orbitals and occupancies (occupied in bold) for the Ph-substituted species **I**. (a) π-type on the ligand, (b) π^*-type on the ligand, (c) $d_{x2\text{-}y2}$-type on Fe, and (d) d_{z2}-type on Fe. The isocontour value is 0.1. H-atoms are omitted for clarity.

be put into direct correspondence with the π-type HOMO and π^*-type LUMO of the free ligand. In addition to the ligand's EFOs, one can also identify two *d*-type EFOs of the metal with the right symmetry, namely a hybrid d_{x2-y2}-type (Figure 3c) and a hybridd_{z2}-type (Figure 3d). As shown in Figure 3, their occupancies are complementary, so one can consider these EFOs as a matching pair. Thus, one can identify a very large charge transfer from the metal onto the LUMO of the cyclopentadienone ligand, which upon coordination exhibits an occupation of 0.411. The *d*-type EFO that donates the charge is also involved in the σ-type interaction with the CO ligand, which also explains its activation. At the same time, another channel is identified where the HOMO of the ligand donates charge to a formally empty *d*-type orbital of the metal, which now exhibits an occupation of 0.361, thus almost balancing the net charge on both moieties. As a result of the metal−ligand interaction, up to three π-type orbitals are (partially) occupied on the five-membered ring, which explains its aromatic character.

We have analyzed the occupation of the relevant EFOs along the reaction profile for all substituted systems (see Tables S15−S26 of the Supporting Information). A systematic trend of the ligand substitution can be observed concerning the occupation of the EFOs of Figure 3a,c along the reaction profile. The replacement of the R_1 = Ph substituent by an EWG such as $R_1 = CF_3$ or $R_1 = NO_2$ induces an increase in the ligand's EFO occupation and a concomitant decrease of the *d*-type EFO occupation of the metal. On the contrary, the presence of EDG causes the opposite effect. The substitution effect on the occupation of the EFOs, as shown in Figure 3b,d, is much less relevant. As a result, the effect of including an electron-donating/-withdrawing group to the ligand is to induce an increase/decrease of the net population on the metal and thus a decrease/increase of its partial atomic charge.

Indeed, a significant correlation is observed between the barrier height of the catalyst activation step and the partial charge of the ligand of both the **I** and **II** species (particularly better for the latter, as shown in Figure 4). The correlation

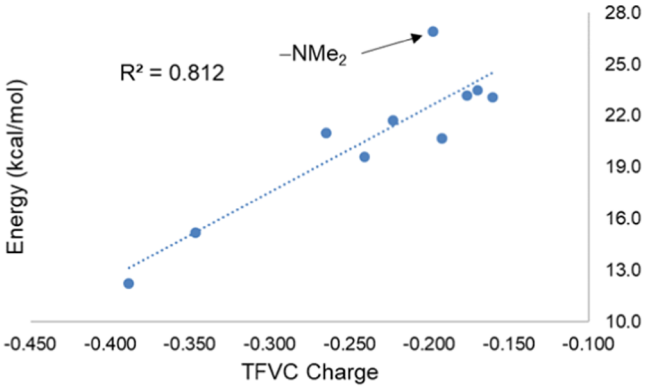

Figure 4. Correlation between the **I** → **II** energy barrier (*y*-axis) and the partial charge of the cyclopentadienone ligand (*x*-axis) in **II**.

further improves discarding the $R_1 = NMe_2$ substituent, for which noticeable steric clashes were found in the **I**−**II** structure (*vide supra*). The barrier height also correlates rather well with the metal's partial charge, but the (indirect) substituent effect on it is more modest. It is worth noticing that the NPA charges on the Fe center are very large and negative, in particular for structure **I** (*ca.* −1.5*e*). With the real-space topological fuzzy voronoi cell (TFVC) approach, the charges obtained (see Table 3) are more chemically appealing (*ca.* +0.8*e*), but essentially the same trends can also be established with NPA charges.

Moving now to the catalytic cycle, the energy barrier of the first step, which corresponds to the entrance of molecular hydrogen to the system by π-bonding to the metallic center, is less kinetically demanding than the previously discussed catalyst activation (see Table 1). The barriers from **II** to **II**−**III** amount *ca.* 5 kcal/mol on average and the substitution induces no noticeable effect.

In the second step, the H−H bond cleavage leads to a H transferred to the carbonyl group of the cyclopentadienone ligand and to the formation of a Fe−H bond. Without the assistance of an explicit molecule, the barrier from **III** → **IV** amounts *ca.* 30 kcal/mol on average. Interestingly, the presence of substituents leads to higher barriers as compared to the original complex **1**, disregarding the electron-donating/-withdrawing character. As can be seen in Table 1, the main effect on the barrier is the destabilization of the TS **III**−**IV**

https://doi.org/10.1021/acs.organomet.2c00099
Organometallics 2022, 41, 1204−1215

structure, which can be as high as 5.0 kcal/mol for R_1 = OH or 5.5 kcal/mol for R_1 = CF_3.

However, when assisted by either an ethanol or a water molecule (see Table 1), the energy barrier for step **III** → **IV** is largely reduced, and with most substituents (excepting NPh_2, CF_3, and NO_2) lying below the barrier for the catalyst activation (**I** and **II**). While the barrier of the nonassisted process does not have a clear relationship with the electronic or steric features of the substituents, the observed reduction of the **III**−**IV** barrier, when assisted by EtOH, seems to follow the same trend as the barrier for step **I**−**II**. That is, introducing an EWG induces a larger decrease of the barrier (−17.2 and −13.9 kcal/mol for R_1 = NO_2 and R_1 = CF_3, respectively) as compared to using an EDG. Still, this effect cannot overcome the destabilization of the TS **III**−**IV** structure upon substitution and thus the lowest ethanol-assisted barrier is found for species **1**, almost isoenergetic with that of the NO_2 substituted ligand.

Following the suggestion of one of the reviewers, we also analyzed the electronic effect of a much smaller EWG such as R_1 = CN in the key steps of the reaction. The results indicate an ethanol-assisted **III**−**IV** barrier of 16.1 kcal/mol, a value in between those obtained for R_1 = NO_2 and R_1 = CF_3. Moreover, the reduction of the barrier due to the solvent molecule amounts to −14.4 kcal/mol, once again in line with that observed for the other EWGs. These findings further point toward the genuine electronic effect of the EWG on the key steps of the catalytic cycle and the catalyst activation.

Finally, the barrier for the last step of the catalytic process (**V** → **VI**) is rather small (*ca.* 5.0 kcal/mol on average), which makes it less interesting. Yet, an inspection of Table 1 again indicates that the presence of EWG on the ligand affords a substantial lowering of the barrier, down to *ca.* 2 kcal/mol for R_1 = NO_2 and R_1 = CF_3.

The energetics of the above-mentioned competitive species **VI'** is also affected by ligand substitution. The coordinated hydrogenation product is lower in energy with respect to the hydrogen-bonded species **VI** by 13.4 kcal/mol (R_1 = OH) to 17.5 kcal/mol (R_1 = CF_3). The stability is somewhat higher with EWG, with 16.0 (R_1 = NO_2) and 16.3 kcal/mol (R_1 = CN) as compared to 14.4 kcal/mol (R_1 = H) and 13.6 (R_1 = Ph) for the reference systems. This trend can be explained by an enhanced Lewis acidity of the Fe center by the presence of an EWG on the ligand. Indeed, the partial charge on Fe for species **II** is the largest for R_1 = CF_3, NO_2 and tends to decrease with respect to R_1 = Ph when introducing EDGs. In addition, knowing that the coordination of alcohols is less favored than amines,[32,40,41] in detail here by 10.6 kcal/mol for the H-substituted catalyst with ethanol, the latter are neither limiting, but competitive.

From the results of intermediate **VI'** and the coordination of EtOH, we can conclude that the barrier-lowering induced by EWG, especially in the activation step (6−7 kcal/mol), is larger than the enhanced stability of these competing intermediates by introducing EWGs (2−3 kcal/mol).

On the other hand, the significant electronic effect observed by introducing EWG such as R_1 = CF_3 and particularly R_1 = NO_2 might also be translated to changes in the formal oxidation states of the metal and the ligands (formal charge) along the catalytic cycle. To answer this question and also to further characterize the different steps of the catalytic cycle,[36b,41] we have performed EOS analysis on all structures along the catalytic cycle (see Tables S16−S25 of the Supporting Information). Structure **I** is best described as neutral Fe(0) species. Both the cyclopentadienone and the CO ligands are also neutral (with a 0 OS). The frontier EFOs for the OS assignation are those shown in Figure 3d,b. As mentioned above, there is a huge charge transfer from the *d*-type EFO of the metal onto the π-type EFO of the ligand, which is responsible for the rather low $R(\%)$ values systematically obtained for the OS assignation. This charge transfer is further enhanced at the TS structure **I**−**II**, and hence in some cases, it is sufficient to consider a transient formal oxidation of the metal. The electron-deficient structure **II** is consistently identified by EOS as Fe(0), with high $R(\%)$ values, while structure **III** is electronically very similar to **I**.

The step **III** → **IV** is the most relevant from the OS point of view. Here, the H_2 ligand is cleaved and H is transferred to the carboxyl group of the cyclopentadienone ligand. The EOS analysis on the TS structure already indicates the oxidation of the metal to a formal Fe(+2), motivated again by an increase of the charge transfer to the π system of the ligand. Such charge transfer is smaller when assisted by an ethanol molecule. Thus, the decrease of the barrier can be connected with a smaller electron reorganization taking place.

Once the cleavage of H_2 is completed to form structure **IV**, a major electron reorganization takes place. First of all, the EOS analysis pictures the H ligand as a (−1) hydride. The electron density donated to the Fe is then transferred to the π system of the cyclopentadienone ligand through the EFOs depicted in Figure 3b,c. Now, the occupation of the π EFO of the ligand is significantly larger than that of the *d*-type EFO of the metal, so that a formal 2e oxidation of the metal to Fe(+2) takes place. Here, the EWG substituents on the ligand promote this electron transfer and more effectively withdraw electrons from the metal (see Tables S16−S25). On the other hand, the proton transferred to the carbonyl partially compensates for the charge on the ligand, which now becomes formally anionic (−1), bearing 6π electrons on the five-membered ring. The rather low $R(\%)$ values obtained for the OS assignation of structure **IV** are due to the marked covalent character of the newly formed Fe−H bond.

CONCLUSIONS

The reductive amination pathway catalyzed by iron-based Knölker derivative catalysts has been thoroughly studied by DFT methods. On the one hand, we found that the proton transfer to the keto group of the cyclopentadienone ligand can be efficiently assisted by an explicit ethanol molecule, leading to a major decrease of the barrier for this step. Thus, the rds of the catalytic pathway, defined by the proton transfer of the **III**−**IV** step, is kinetically less demanding than the catalyst preactivation (**I**−**II**), *i.e.*, the first CO release assisted by Me_3NO, with an energy of 19.6 kcal/mol (for the phenyl-substituted complex). In addition, a computational screening of the substituent effect on the cyclopentadienone ligand has been carried out. We found that the presence of electron-withdrawing groups induces a decrease in the activation barriers of the most relevant steps, namely the first CO release and the H_2 cleavage and subsequent proton transfer. In particular, there is an important decrease with the substitution of phenyl groups by $-NO_2$, where we obtain an energy barrier of 12.2 kcal/mol, thus the latter being the most energetically demanding step for this system, as well as for the $-CF_3$ one. Structural and in-depth electronic characterization of the species indicates that the cyclopentadienone ligand is more

https://doi.org/10.1021/acs.organomet.2c00099
Organometallics 2022, 41, 1204−1215

than a simple spectator. We have identified persistent changes in the planarity of the five-membered ring along the catalytic cycle, which are not translated into changes in its aromaticity. Thus, the nonaromatic free ligand becomes aromatic upon complex formation and shows a rather constant aromatic character along the reaction that is not modulated by the substituents. The effective fragment orbitals (EFOs) of the metal and ligand allows the monitoring of the electron flow between the moieties along the catalytic cycle and a better assessment of the actual substituent effects. The net effect of including an electron-donating/-withdrawing group to the ligand is to induce an increase/decrease of the net population on the metal and at the same time a decrease/increase of the π density of the ring. A good correlation of the ligand's charge with the barrier height of the first step has been established. Our theoretical studies provide a better understanding of the effect of the substituents and will help to develop more efficient catalysts.

COMPUTATIONAL DETAILS

All calculations were performed at the DFT level with the Gaussian09 set of programs,[42] using the BP86 and M06 functionals.[43] The electronic configuration of the molecular systems was described with the standard split-valence basis set with a polarization function of Ahlrichs and co-workers for H, C, N, O, and F (SVP keyword in Gaussian).[44] For Fe, the quasi-relativistic Stuttgart/Dresden effective core potential[45] with an associated valence basis set (standard SDD keywords in Gaussian09) was used. Geometry optimizations were carried out without symmetry constraints and normal mode analysis were computed to confirm minima on the potential energy surface. These frequencies were used to calculate unscaled zero-point energies (ZPEs) as well as thermal corrections and entropy effects at 298 K and 1 atm using the standard statistical mechanics relationships for an ideal gas. Accurate electronic energies were obtained *via* single-point calculation on the BP86-optimized geometries using the M06 functional.[46] In these calculations, the cc-pVTZ basis set was used for describing H, C, N, O, and F,[47] whereas for Fe, the SDD basis set (and pseudopotential) has been employed, together with the solvent effects of ethanol estimated with the polarizable continuous solvation model (PCM).[48,49] On top of the M06/cc-pVTZ—SDD(pcm-EtOH) electronic energies, we added the thermal and entropy corrections obtained (gas-phase) at the BP86/SVP—SDD level.

Aromaticity was evaluated using the magnetic indicator nucleus-independent chemical shift (NICS),[50,51] proposed by Schleyer and co-workers. NICS is defined as the negative value of the absolute shielding and typically is evaluated at the ring center (NICS(0)) and/or at 1 Å above ($NICS(1)_{out}$) or below ($NICS(1)_{in}$). The ring center of the nonplanar five-membered ring has been obtained by adjusting the best fitting plane passing through the respective nuclei in a least-squares sense.[52,53] NICS values were computed by locating ghost atoms in the aforementioned points at the BP86/6-31+G**//BP86/SVP—SDD level and using the gauge-including atomic orbital method (GIAO).

Metal and ligand oxidation states (OS) were elucidated with the effective oxidation states (EOS) analysis method, which relies on Mayer's effective fragment orbitals (EFOs) and their associated occupations. The EFOs are sorted by decreasing the occupation number and then individual electrons (or pairs for closed-shell wavefunctions) are assigned to those with higher occupations, thus considering each EFO as occupied or empty. This leads to an effective configuration of the atoms/ligands within the molecule, which directly determines their OS. The difference between the occupation number of the last occupied (λ^{σ}_{LO}) and the first unoccupied (λ^{σ}_{FU}) EFOs is a pointer of how clear-cut the assignment has been performed. The larger this difference, the better the current electron distribution can be pictured into a discrete ionic model. Thus, the EOS analysis provides the OS of the fragments/atoms desired together with its reliability index ($R = \min(R_{\alpha}R_{\beta})$), defined for each spin case σ as

$$R_{\sigma}(\%) = 100\cdot\min(1, \max(0, \lambda^{\sigma}_{LO} - \lambda^{\sigma}_{FU} + 1/2)) \quad (1)$$

The worst-case scenario is when two or more frontier EFOs sitting on different fragments exhibit the same occupation number. In these cases, two different OS distributions with $R(\%) = 50$ are equally plausible. EOS analysis has been performed at the M06/cc-pVTZ—SDD(pcm-EtOH)//BP86/SVP—SDD level of theory with the in-house developed program APOST-3D,[38] using the topological fuzzy voronoi cell (TFVC) atomic definition[54] and a 40 × 146 atomic grid for the numerical integrations.

ASSOCIATED CONTENT

Supporting Information

The Supporting Information is available free of charge at https://pubs.acs.org/doi/10.1021/acs.organomet.2c00099.

Electronic and Gibbs energies collected for each species (Tables S1−S11), aromaticity and EOS analysis (Tables S12−S24), planarity evaluation of the cyclopentadienone (Table S26), and the NPA charges on iron (Table S27) (PDF)

XYZ coordinates of all studied systems (XYZ)

AUTHOR INFORMATION

Corresponding Authors

Jean-Luc Renaud − *Normandie Univ, LCMT, ENSICAEN, UNICAEN, CNRS, 14000 Caen, France;* orcid.org/0000-0001-8757-9622; Email: jean-luc.renaud@ensicaen.fr

Pedro Salvador − *Institut de Química Computacional i Catàlisi and Departament de Química, Universitat de Girona, 17003 Girona, Catalonia, Spain;* orcid.org/0000-0003-1823-7295; Email: pedro.salvador@udg.edu

Albert Poater − *Institut de Química Computacional i Catàlisi and Departament de Química, Universitat de Girona, 17003 Girona, Catalonia, Spain;* orcid.org/0000-0002-8997-2599; Email: albert.poater@udg.edu

Authors

Martí Gimferrer − *Institut de Química Computacional i Catàlisi and Departament de Química, Universitat de Girona, 17003 Girona, Catalonia, Spain;* orcid.org/0000-0001-5222-2201

Nicolas Joly − *Institut de Química Computacional i Catàlisi and Departament de Química, Universitat de Girona, 17003 Girona, Catalonia, Spain; Normandie Univ, LCMT, ENSICAEN, UNICAEN, CNRS, 14000 Caen, France*

Sílvia Escayola − *Institut de Química Computacional i Catàlisi and Departament de Química, Universitat de Girona, 17003 Girona, Catalonia, Spain; Donostia*

https://doi.org/10.1021/acs.organomet.2c00099
Organometallics 2022, 41, 1204−1215

International Physics Center (DIPC), 20018 Donostia, Euskadi, Spain; orcid.org/0000-0002-1159-7397

Eduard Viñas − *Institut de Química Computacional i Catàlisi and Departament de Química, Universitat de Girona, 17003 Girona, Catalonia, Spain*

Sylvain Gaillard − *Normandie Univ, LCMT, ENSICAEN, UNICAEN, CNRS, 14000 Caen, France;* orcid.org/0000-0003-3402-2518

Miquel Solà − *Institut de Química Computacional i Catàlisi and Departament de Química, Universitat de Girona, 17003 Girona, Catalonia, Spain;* orcid.org/0000-0002-1917-7450

Complete contact information is available at: https://pubs.acs.org/10.1021/acs.organomet.2c00099

Author Contributions

All authors have given approval to the final version of the manuscript.

Notes

The authors declare no competing financial interest.

■ ACKNOWLEDGMENTS

S.G., N.J., and J.-L.R. gratefully acknowledge financial support from the "Ministère de la Recherche et des Nouvelles Technologies", Normandie Université, CNRS, and the LABEX SynOrg (ANR-11-LABX-0029). N.J. acknowledges the Graduate School of Research XL-Chem (ANR-18-EURE-0020 XL-Chem) for the PhD fellowship. A.P., P.S., and M.S. thank the Ministerio de Economía y Competitividad (MINECO) of Spain for projects PGC2018-097722-B-I00, PGC2018-098212-B-C22, and PID2020-13711GB-I00 and Generalitat de Catalunya for projects 2017SGR39 and ICREA Academia prize 2019. A.P. is a Serra Húnter fellow. M.G. thanks the Generalitat de Catalunya and Fons Social Europeu for the predoctoral fellowship (2018 FI_B01120). S.E. thanks Universitat de Girona and Donostia International Physics Center (DIPC) for an IFUdG2019 predoctoral fellowship. They also thank all of the referees for their helpful comments and suggestions.

■ REFERENCES

(1) Parshall, G. W.; Steven, D. I. In Homogeneous Catalysis. In *The Applications and Chemistry of Catalysis by Soluble Transition Metal Complexes*; Wiley: New York, 1992; pp 25−50.

(2) Huo, C.-F.; Li, Y.-W.; Beller, M.; Jiao, H. Catalyzed Chemoselective Acrolein Hydrogenation. Density Functional Studies. *Organometallics* **2004**, *23*, 2168−2178.

(3) Ohkuma, T.; Ooka, H.; Ikariya, T.; Noyori, R. Preferential hydrogenation of aldehydes and ketones. *J. Am. Chem. Soc.* **1995**, *117*, 10417−10418.

(4) Klingler, F. D. Asymmetric Hydrogenation of Prochiral Amino Ketones to Amino Alcohols for Pharmaceutical Use. *Acc. Chem. Res.* **2007**, *40*, 1367−1376.

(5) (a) El-Sepelgy, O.; Alandini, N.; Rueping, M. Merging Iron Catalysis and Biocatalysis—Iron Carbonyl Complexes as Efficient Hydrogen Autotransfer Catalysts in Dynamic Kinetic Resolutions. *Angew. Chem., Int. Ed.* **2016**, *55*, 13602−13605. (b) El-Sepelgy, O.; Brzozowska, A.; Azofra, L. M.; Jang, Y. K.; Cavallo, L.; Rueping, M. Experimental and Computational Study of an Unexpected Iron-Catalyzed Carboetherification by Cooperative Metal and Ligand Substrate Interaction and Proton Shuttling. *Angew. Chem., Int. Ed.* **2017**, *56*, 14863−14867.

(6) For some examples, see: (a) Ikenaga, T.; Matsushita, K.; Shinozawa, J.; Yada, S.; Takagi, Y. The Effects of Added Ammonium Chloride in The Reductive Amination of Some Carbonyl Compounds over Ru and Pd Catalysts. *Tetrahedron* **2005**, *61*, 2105−2109. (b) Falus, P.; Boros, Z.; Hornyanszky, G.; Nagy, J.; Darvas, F.; Ürge, L.; Poppe, L. Reductive Amination of Ketones: Novel One-Step Transfer Hydrogenations in Batch and Continuous-Flow Mode. *Tetrahedron Lett.* **2011**, *52*, 1310−1312. (c) Wei, D.; BruneauVoisine, A.; Valyaev, D. A.; Lugan, N.; Sortais, J.-B. Manganese catalyzed reductive amination of aldehydes using hydrogen as a reductant. *Chem. Commun.* **2018**, *54*, 4302−4305. and references cited therein For pioneer work in iron-catalysis, see: (d) Fleischer, S.; Zhou, S.; Junge, K.; Beller, M. An Easy and General Iron-catalyzed Reductive Amination of Aldehydes and Ketones with Anilines. *Chem. - Asian J.* **2011**, *6*, 2240−2245. (e) Bhor, M. D.; Bhanushali, M. J.; Nandurkar, N. S.; Bhanage, B. M. Direct reductive amination of carbonyl compounds with primary/secondary amines using recyclable water-soluble Fe^{II}/EDTA complex as catalyst. *Tetrahedron Lett.* **2008**, *49*, 965−969.

(7) For some recent examples, see: (a) Wang, C.; Pettman, A.; Basca, J.; Xiao, J. A Versatile Catalyst for Reductive Amination by Transfer Hydrogenation. *Angew. Chem., Int. Ed.* **2010**, *49*, 7548−7552. (b) Huang, Y.-B.; Dai, J.-J.; Deng, X.-J.; Qu, Y.-C.; Guo, Q.-X.; Fu, Y. Ruthenium-Catalyzed Conversion of Levulinic Acid to Pyrrolidines by Reductive Amination. *ChemSusChem* **2011**, *4*, 1578−1581. (c) Wang, S.; Huang, H.; Bruneau, C.; Fischmeister, C. Selective and Efficient Iridium Catalyst for the Reductive Amination of Levulinic Acid into Pyrrolidones. *ChemSusChem* **2017**, *10*, 4150−4154. (d) Wei, Y.; Wang, C.; Jiang, X.; Xue, D.; Li, J.; Xiao, J. Highly Efficient Transformation of Levulinic Acid into Pyrrolidinones by Iridium Catalysed Transfer Hydrogenation. *Chem. Commun.* **2013**, *49*, 5408−5410. (e) Zhu, M. Ruthenium-Catalyzed Direct Reductive Amination in $HCOOH/NEt_3$ Mixture. *Catal. Lett.* **2014**, *144*, 1568−1572. (f) Yang, P.; Lim, L. H.; Chuanprasit, P.; Hirao, H.; Zhou, J. S. Nickel-Catalyzed Enantioselective Reductive Amination of Ketones with Both Arylamines and Benzhydrazide. *Angew. Chem., Int. Ed.* **2016**, *55*, 12083−12087. (g) Metzker, G.; Dias, R. M. P.; Burtoloso, A. C. B. Iron-Catalyzed Reductive Amination from Levulinic and Formic Acid Aqueous Solutions: An Approach for the Selective Production of Pyrrolidones in Biorefinery Facilities. *ChemistrySelect* **2018**, *3*, 368−372.

(8) (a) Gnanamgari, D.; Moores, A.; Rajaseelan, E.; Crabtree, R. H. Transfer Hydrogenation of Imines and Alkenes and Direct Reductive Amination of Aldehydes Catalyzed by Triazole-Derived Iridium(I) Carbene Complexes. *Organometallics* **2007**, *26*, 1226−1230. (b) Dou, X.; Hayashi, T. Synthesis of Planar Chiral Shvo Catalysts for Asymmetric Transfer Hydrogenation. *Adv. Synth. Catal.* **2016**, *358*, 1054−1058. For examples in iron chemistry, see: (c) Vayer, M.; Morcillo, S. P.; Dupont, J.; Gandon, V.; Bour, C. Iron-Catalyzed Reductive Ethylation of Imines with Ethanol. *Angew. Chem., Int. Ed.* **2018**, *57*, 3228−3232. (d) Zhou, S.; Fleischer, S.; Junge, K.; Das, S.; Addis, D.; Beller, M. Enantioselective Synthesis of Amines: General, Efficient Iron-Catalyzed Asymmetric Transfer Hydrogenation of Imines. *Angew. Chem., Int. Ed.* **2010**, *49*, 8121−8125. (e) Facchini, S. V.; Cettolin, M.; Bai, X.; Casamassima, G.; Pignataro, L.; Gennari, C.; Piarulli, U. Efficient Synthesis of Amines by Iron-Catalyzed C═N Transfer Hydrogenation and C═O Reductive Amination. *Adv. Synth. Catal.* **2018**, *360*, 1054−1059. (f) Coufourier, S.; Ndiaye, D.; Gaignard Gaillard, Q.; Bettoni, L.; Joly, N.; Mbaye, M. D.; Poater, A.; Gaillard, S.; Renaud, J.-L. Iron-catalyzed chemoselective hydride transfer reactions. *Tetrahedron* **2021**, *90*, No. 132187. (g) Petricci, E.; Santillo, N.; Castagnolo, D.; Cini, E.; Taddei, M. Iron-Catalyzed Reductive Amination of Aldehydes in Isopropyl Alcohol/Water Media as Hydrogen Sources. *Adv. Synth. Catal.* **2018**, *360*, 2560−2565.

(9) For selected reviews: (a) Bähn, S.; Imm, S.; Neubert, L.; Zhang, M.; Neumann, H.; Beller, M. The Catalytic Amination of Alcohols. *ChemCatChem* **2011**, *3*, 1853−1864. (b) Yang, Q.; Wang, Q.; Yu, Z. Substitution of Alcohols by N-Nucleophiles via Transition Metal-Catalyzed Dehydrogenation. *Chem. Soc. Rev.* **2015**, *44*, 2305−2329. (c) Renaud, J.-L.; Gaillard, S. Recent Advances in Iron- and Cobalt-

Complex-Catalyzed Tandem/Consecutive Processes Involving Hydrogenation. *Synthesis* **2016**, *48*, 3659−3683. (d) Quintard, A.; Rodriguez, J. A Step into an eco-Compatible Future: Iron- and Cobalt-catalyzed Borrowing Hydrogen Transformation. *ChemSusChem* **2016**, *9*, 28−30.

(10) For some recent articles on iron complexes-catalyzed amine alkylation: (a) Yan, T.; Feringa, B. L.; Barta, K. Iron Catalysed Direct Alkylation of Amines with Alcohols. *Nat. Commun.* **2014**, *5*, No. 5602. (b) Yan, T.; Feringa, B. L.; Barta, K. Benzylamines via Iron-Catalyzed Direct Amination of Benzyl Alcohols. *ACS Catal.* **2016**, *6*, 381−388. (c) Yan, T.; Feringa, B. L.; Barta, K. Direct N-alkylation of unprotected amino acids with alcohols. *Sci. Adv.* **2017**, *3*, No. eaao6494. (d) Mastalir, M.; Stöger, B.; Pittenauer, E.; Puchberger, M.; Allmaries, G.; Kirchner, G. Air Stable Iron(II) PNP Pincer Complexes as Efficient Catalysts for the Selective Alkylation of Amines with Alcohols. *Adv. Synth. Catal.* **2016**, *358*, 3824−3831. (e) Brown, T. J.; Cumbes, M.; Diorazio, L. J.; Clarkson, G. J.; Wills, M. Use of (Cyclopentadienone)iron Tricarbonyl Complexes for C-N Bond Formation Reactions between Amines and Alcohols. *J. Org. Chem.* **2017**, *82*, 10489−10503. (f) Pan, H.-J.; Ng, T. W.; Zhao, Y. Iron-Catalyzed Amination of Alcohols Assisted by Lewis Acid. *Chem. Commun.* **2015**, *51*, 11907−11910. (g) Polidano, K.; Allen, B. D. W.; Williams, J. M. J.; Morrill, L. C. Iron-Catalyzed Methylation Using the Borrowing Hydrogen Approach. *ACS Catal.* **2018**, *8*, 6440−6445. (h) Lator, A.; Gaillard, S.; Poater, A.; Renaud, J.-L. Well-Defined Phosphine-Free Iron-Catalyzed N-Ethylation and N-Methylation of Amines with Ethanol and Methanol. *Org. Lett.* **2018**, *20*, 5985−5990. (i) Joly, N.; Bettoni, L.; Gaillard, S.; Poater, A.; Renaud, J.-L. Phosphine-free ruthenium complex-catalyzed synthesis of mono- or dialkylated acyl hydrazides via the borrowing hydrogen strategy. *J. Org. Chem.* **2021**, *86*, 6813−6825. (j) Bettoni, L.; Joly, N.; Lohier, J.-F.; Gaillard, S.; Poater, A.; Renaud, J.-L. Ruthenium-Catalyzed Three-Component Alkylation: A Tandem Approach to the Synthesis of Nonsymmetric *N,N*-Dialkyl Acyl Hydrazides with Alcohols. *Adv. Synth. Catal.* **2021**, *363*, 4009−4017.

(11) Zhou, Q.-L.; Xie, J.-H. Transition metal-catalyzed enantioselective hydrogenation of enamides and enamines. *Top. Curr. Chem.* **2014**, *343*, 75−101.

(12) (a) Noyori, R.; Umeda, I.; Ishigami, T. Selective hydrogenation of α,β-unsaturated carbonyl compounds via hydridoiron complexes. *J. Org. Chem.* **1972**, *37*, 1542−1545. (b) Lee, H.-Y.; An, M. Selective 1,4-reduction of unsaturated carbonyl compounds using $Co_2(CO)_8$−H_2O. *Tetrahedron Lett.* **2003**, *44*, 2775−2778.

(13) Shvo, Y.; Czarkie, D.; Rahamim, Y.; Chodosh, D. F. A new group of ruthenium complexes: structure and catalysis. *J. Am. Chem. Soc.* **1986**, *108*, 7400−7402.

(14) (a) Privalov, T.; Samec, J. S. M.; Bäckvall, J.-E. DFT Study of an Inner-Sphere Mechanism in the Hydrogen Transfer from a Hydroxycyclopentadienyl Ruthenium Hydride to Imines. *Organometallics* **2007**, *26*, 2840−2848. (b) Comas-Vives, A.; Ujaque, G.; Lledós, A. Hydrogen Transfer to Ketones Catalyzed by Shvo's Ruthenium Hydride Complex: A Mechanistic Insight. *Organometallics* **2007**, *26*, 4135−4144. (c) Comas-Vives, A.; Ujaque, G.; Lledós, A. Theoretical Analysis of the Hydrogen-Transfer Reaction to C═N, C═C, and C≡C Bonds Catalyzed by Shvo's Ruthenium Complex. *Organometallics* **2008**, *27*, 4854−4863.

(15) (a) Casey, C. P.; Guan, H. An Efficient and Chemoselective Iron Catalyst for the Hydrogenation of Ketones. *J. Am. Chem. Soc.* **2007**, *129*, 5816−5817. (b) Casey, C. P.; Guan, H. Cyclopentadienone Iron Alcohol Complexes: Synthesis, Reactivity, and Implications for the Mechanism of Iron-Catalyzed Hydrogenation of Aldehydes. *J. Am. Chem. Soc.* **2009**, *131*, 2499−2507.

(16) Knölker, H.-J.; Baum, E.; Goesmann, H.; Klauss, R. Demetalation of Tricarbonyl(cyclopentadienone)iron Complexes Initiated by a Ligand Exchange Reaction with NaOH-X-Ray Analysis of a Complex with Nearly Square-Planar Coordinated Sodium. *Angew. Chem., Int. Ed.* **1999**, *38*, 2064−2066.

(17) (a) Elangovan, S.; Topf, C.; Fischer, S.; Jiao, H.; Spannenberg, A.; Baumann, W.; Ludwig, R.; Junge, K.; Beller, M. Selective Catalytic Hydrogenations of Nitriles, Ketones, and Aldehydes by Well-Defined Manganese Pincer Complexes. *J. Am. Chem. Soc.* **2016**, *138*, 8809−8814. (b) Rösler, S.; Obenauf, J.; Kempe, R. A Highly Active and Easily Accessible Cobalt Catalyst for Selective Hydrogenation of C═O Bonds. *J. Am. Chem. Soc.* **2015**, *137*, 7998−8001.

(18) (a) Bauer, I.; Knölker, H.-J. Iron Catalysis in Organic Synthesis. *Chem. Rev.* **2015**, *115*, 3170−3387. (b) Gopalaiah, K. Chiral Iron Catalysts for Asymmetric Synthesis. *Chem. Rev.* **2013**, *113*, 3248−3296. (c) Bullock, R. M. Abundant Metals Give Precious Hydrogenation Performance. *Science* **2013**, *342*, 1054−1055. (d) Mérel, D. S.; Do, M. L. T.; Gaillard, S.; Dupau, P.; Renaud, J.-L. Iron-catalyzed reduction of carboxylic and carbonic acid derivatives. *Coord. Chem. Rev.* **2015**, *288*, 50−68. (e) Dupau, P.; Do, M. L. T.; Gaillard, S.; Renaud, J.-L. Iron-Catalyzed Hydrogenation of Esters to Alcohols. *Angew. Chem., Int. Ed.* **2014**, *53*, 13004−13006. (f) Sues, P. E.; Demmans, K. Z.; Morris, R. H. Rational development of iron catalysts for asymmetric transfer hydrogenation. *Dalton Trans.* **2014**, *43*, 7650−7667. (g) Greenhalgh, M. D.; Jones, A. S.; Thomas, S. P. Iron-Catalysed Hydrofunctionalisation of Alkenes and Alkynes. *ChemCatChem* **2015**, *7*, 190−222. (h) Zell, T.; Milstein, D. Hydrogenation and Dehydrogenation Iron Pincer Catalysts Capable of Metal−Ligand Cooperation by Aromatization/Dearomatization. *Acc. Chem. Res.* **2015**, *48*, 1979−1994. (i) Morris, R. H. Exploiting Metal−Ligand Bifunctional Reactions in the Design of Iron Asymmetric Hydrogenation Catalysts. *Acc. Chem. Res.* **2015**, *48*, 1494−1502. (j) Misal Castro, L. C.; Li, H.; Sortais, J.-B.; Darcel, C. When iron met phosphines: a happy marriage for reduction catalysis. *Green Chem.* **2015**, *17*, 2283−2303. (k) Bigler, R.; Huber, R.; Mezzetti, A. Iron Chemistry Made Easy: Chiral N_2P_2 Ligands for Asymmetric Catalysis. *Synlett* **2016**, *27*, 831−847. (l) McNeill, E.; Ritter, T. 1,4-Functionalization of 1,3-Dienes With Low-Valent Iron Catalysts. *Acc. Chem. Res.* **2015**, *48*, 2330−2343.

(19) (a) Liu, J.; Song, Y.; Ma, L. Earth-abundant Metal-catalyzed Reductive Amination: Recent Advances and Prospect for Future Catalysis. *Chem. - Asian J.* **2021**, *16*, 2371−2391. (b) Irrgang, T.; Kempe, R. Transition-metal-catalyzed reductive amination employing hydrogen. *Chem. Rev.* **2020**, *120*, 9583−9674.

(20) (a) Mérel, D. S.; Elie, M.; Lohier, J.-F.; Gaillard, S.; Renaud, J.-L. Bifunctional Iron Complexes: Efficient Catalysts for C═O and C═N Reduction in Water. *ChemCatChem* **2013**, *5*, 2939−2945. (b) Pagnoux-Ozherelyeva, A.; Pannetier, N.; Mbaye, D. M.; Gaillard, S.; Renaud, J.-L. Knölker's Iron Complex: An Efficient In Situ Generated Catalyst for Reductive Amination of Alkyl Aldehydes and Amines. *Angew. Chem.* **2012**, *51*, 4976−4980.

(21) Moulin, S.; Dentel, H.; Pagnoux-Ozherelyeva, A.; Gaillard, S.; Poater, A.; Cavallo, L.; Lohier, J.-F.; Renaud, J.-L. Bifunctional (Cyclopentadienone)Iron−Tricarbonyl Complexes: Synthesis, Computational Studies and Application in Reductive Amination. *Chem. - Eur. J.* **2013**, *19*, 17881−17890.

(22) Thai, T.-T.; Mérel, D. S.; Poater, A.; Gaillard, S.; Renaud, J.-L. Highly Active Phosphine-Free Bifunctional Iron Complex for Hydrogenation of Bicarbonate and Reductive Amination. *Chem. - Eur. J.* **2015**, *21*, 7066−7070.

(23) (a) Fleischer, S.; Zhou, S.; Junge, K.; Beller, M. General and Highly Efficient Iron-Catalyzed Hydrogenation of Aldehydes, Ketones, and α,β-Unsaturated Aldehydes. *Angew. Chem., Int. Ed.* **2013**, *52*, 5120−5124. (b) Gorgas, N.; Stöger, B.; Veiros, L. F.; Kirchner, K. Highly Efficient and Selective Hydrogenation of Aldehydes: A Well-Defined Fe(II) Catalyst Exhibits Noble-Metal Activity. *ACS Catal.* **2016**, *6*, 2664−2672. (c) Mazza, S.; Scopelliti, R.; Hu, X. Chemoselective Hydrogenation and Transfer Hydrogenation of Aldehydes Catalyzed by Iron(II) PONOP Pincer Complexes. *Organometallics* **2015**, *34*, 1538−1545. (d) Wienhöfer, G.; Westerhaus, F. A.; Junge, K.; Ludwig, R.; Beller, M. A Molecularly Defined Iron-Catalyst for the Selective Hydrogenation of α,β-Unsaturated Aldehydes. *Chem. - Eur. J.* **2013**, *19*, 7701−7707.

(24) Coufourier, S.; Gaignard-Gaillard, Q.; Lohier, J.-F.; Poater, A.; Gaillard, S.; Renaud, J.-L. Hydrogenation of CO_2, Hydrogenocar-

https://doi.org/10.1021/acs.organomet.2c00099
Organometallics 2022, 41, 1204−1215

bonate, and Carbonate to Formate in Water using Phosphine Free Bifunctional Iron Complexes. *ACS Catal.* **2020**, *10*, 2108−2116.
(25) Seck, C.; Mbaye, M. D.; Coufourier, S.; Lator, A.; Lohier, J.-F.; Poater, A.; Ward, T. R.; Gaillard, S.; Renaud, J.-L. Alkylation of Ketones Catalyzed by Bifunctional Iron Complexes: From Mechanistic Understanding to Application. *ChemCatChem* **2017**, *9*, 4410−4416.
(26) Amin, S. R.; Crowe, W. E. Reduction of Imines via Titanium-Catalyzed Hydromagnesation. *Tetrahedron Lett.* **1997**, *38*, 7487−7490.
(27) Nugent, T. C.; Ghosh, A. K.; Wakchaure, V. N.; Mohanty, R. R. Asymmetric Reductive Amination: Convenient Access to Enantioenriched Alkyl-Alkyl or Aryl-Alkyl Substituted α-Chiral Primary Amines. *Adv. Synth. Catal.* **2006**, *348*, 1289−1299.
(28) Tadiello, L.; Gandini, T.; Stadler, B. M.; Tin, S.; Jiao, H.; de Vries, J. G.; Pignataro, L.; Gennari, C. Regiodivergent Reductive Opening of Epoxides by Catalytic Hydrogenation Promoted by a (Cyclopentadienone)iron Complex. *ACS Catal.* **2022**, *12*, 235−246.
(29) von der Höh, A.; Berkessel, A. Insight into the Mechanism of Dihydrogen-Heterolysis at Cyclopentadienone Iron Complexes and Subsequent C-X Hydrogenation. *ChemCatChem* **2011**, *3*, 861−867.
(30) Zhang, H.; Chen, D.; Zhang, Y.; Zhanga, G.; Liu, J. On the mechanism of carbonyl hydrogenation catalyzed by iron catalyst. *Dalton Trans.* **2010**, *39*, 1972−1978.
(31) Hackl, L.; Phong Ho, L.; Bockhardt, D.; Bannenberg, T.; Tamm, M. Tetraaminocyclopentadienone Iron Complexes as Hydrogenation Catalysts. *Organometallics* **2022**, *41*, 836−851.
(32) Lu, X.; Cheng, R.; Turner, N.; Liu, Q.; Zhang, M.; Sun, X. High Chemoselectivity of an Advanced Iron Catalyst for the Hydrogenation of Aldehydes with Isolated C═C Bond: A Computational Study. *J. Org. Chem.* **2014**, *79*, 9355−9364.
(33) Lu, X.; Zhang, Y.; Yun, P.; Zhang, M.; Li, T. The mechanism for the hydrogenation of ketones catalyzed by Knölker's iron-catalyst. *Org. Biomol. Chem.* **2013**, *11*, 5264−5277.
(34) Gonçalves, T. P.; Huang, K.-W. Metal-Ligand Cooperative Reactivity in the (Pseudo)-Dearomatized $PN^{x}(P)$ Systems: The Influence of the Zwitterionic Form in Dearomatized Pincer Complexes. *J. Am. Chem. Soc.* **2017**, *139*, 13442−13449.
(35) Pal, R.; Mukherjee, S.; Chandrasekhar, S.; Row, T. N. Exploring Cyclopentadienone Antiaromaticity: Charge Density Studies of Various Tetracyclones. *J. Phys. Chem. A* **2014**, *118*, 3479−3489.
(36) (a) Poater, J.; Gimferrer, M.; Poater, A. Covalent and Ionic Capacity of MOFs To Sorb Small Gas Molecules. *Inorg. Chem.* **2018**, *57*, 6981−6990. (b) Poater, A.; Ribas, X.; Llobet, A.; Cavallo, L.; Solà, M. Complete Mechanism of σ^* Intramolecular Aromatic Hydroxylation through O_2 Activation by a Macrocyclic Dicopper(I) Complex. *J. Am. Chem. Soc.* **2008**, *130*, 17710−17717. (c) Palusiak, M.; Simon, S.; Solà, M. Interplay between intramolecular resonance-assisted hydrogen bonding and local aromaticity. II. 1,3-dihydroxyaryl-2-aldehydes. *J. Org. Chem.* **2009**, *74*, 2059−2066. (d) Richmond, C. J.; Escayola, S.; Poater, A. Axial Ligand effects of Ru-BDA Complexes in the O-O Bond Formation via the I2M Bimolecular Mechanism in Water Oxidation Catalysis. *Eur. J. Inorg. Chem.* **2019**, *2019*, 2101−2108. (e) Masdemont, J.; Luque-Urrutia, J. A.; Gimferrer, M.; Milstein, D.; Poater, A. Mechanism of Coupling of Alcohols and Amines to Generate Aldimines and H_2 by a Pincer Manganese Catalyst. *ACS Catal.* **2019**, *9*, 1662−1669. (f) Chawla, M.; Poater, A.; Oliva, R.; Cavallo, L. Structural and energetic characterization of the emissive RNA alphabet based on the isothiazolo[4,3-d]pyrimidine heterocycle core. *Phys. Chem. Chem. Phys.* **2016**, *18*, 18045−18053.
(37) Salvador, P.; Ramos-Cordoba, E.; Gimferrer, M. *APOST-3D Program*; Universitat de Girona: Girona, Spain, 2019.
(38) Ramos-Córdoba, E.; Postils, V.; Salvador, P. Oxidation States from Wave Function Analysis. *J. Chem. Theory Comput.* **2015**, *11*, 1501−1508.
(39) Postils, V.; Delgado-Alonso, C.; Luis, J. M.; Salvador, P. An Objective Alternative to IUPAC's Approach To Assign Oxidation States. *Angew. Chem., Int. Ed.* **2018**, *57*, 10525−10529.
(40) Lu, X.; Zhang, Y.; Turner, N.; Zhang, M.; Li, T. Using computational methods to explore improvements to Knölker's iron catalyst. *Org. Biomol. Chem.* **2014**, *12*, 4361−4371.
(41) (a) Gimferrer, M.; Salvador, P.; Poater, A. Computational Monitoring of Oxidation States in Olefin Metathesis. *Organometallics* **2019**, *38*, 4585−4592. (b) Gimferrer, M.; Van Der Mynsbrugge, J.; Bell, A. T.; Salvador, P.; Head-Gordon, M. Facing the Challenges of Borderline Oxidation State Assignments Using State-of-the-Art Computational Methods. *Inorg. Chem.* **2020**, *59*, 15410−15420.
(42) Frisch, M. J.; Trucks, G. W.; Schlegel, H. B.; Scuseria, G. E.; Robb, M. A.; Cheeseman, J. R.; Scalmani, G.; Barone, V.; Mennucci, B.; Petersson, G. A.; Nakatsuji, H.; Caricato, M.; Li, X.; Hratchian, H. P.; Izmaylov, A. F.; Bloino, J.; Zheng, G.; Sonnenberg, J. L.; Hada, M.; Ehara, M.; Toyota, K.; Fukuda, R.; Hasegawa, J.; Ishida, M.; Nakajima, T.; Honda, Y.; Kitao, O.; Nakai, H.; Vreven, T.; Montgomery, J. A., Jr.; Peralta, J. E.; Ogliaro, F.; Bearpark, M.; Heyd, J. J.; Brothers, E.; Kudin, K. N.; Staroverov, V. N.; Kobayashi, R.; Normand, J.; Raghavachari, K.; Rendell, A.; Burant, J. C.; Iyengar, S. S.; Tomasi, J.; Cossi, M.; Rega, N.; Millam, J. M.; Klene, M.; Knox, J. E.; Cross, J. B.; Bakken, V.; Adamo, C.; Jaramillo, J.; Gomperts, R.; Stratmann, R. E.; Yazyev, O.; Austin, A. J.; Cammi, R.; Pomelli, C.; Ochterski, J. W.; Martin, R. L.; Morokuma, K.; Zakrzewski, V. G.; Voth, G. A.; Salvador, P.; Dannenberg, J. J.; Dapprich, S.; Daniels, A. D.; Farkas, Ö.; Foresman, J. B.; Ortiz, J. V.; Cioslowski, J.; Fox, D. J. *Gaussian 09*, Revision E.01; Gaussian, Inc.: Wallingford CT, 2009.
(43) (a) Becke, A. D. Density-functional Exchange-Energy Approximation with Correct Asymptotic Behavior. *Phys. Rev. A: At., Mol., Opt. Phys.* **1988**, *38*, 3098−3100. (b) Perdew, J. P. Density-Functional Approximation for the Correlation Energy of the Inhomogeneous Electron Gas. *Phys. Rev. B: Condens. Matter Mater. Phys.* **1986**, *33*, 8822−8824.
(44) Schäfer, A.; Huber, C.; Ahlrichs, R. Fully optimized contracted Gaussian basis sets of triple zeta valence quality for atoms Li to Kr. *J. Chem. Phys.* **1994**, *100*, 5829.
(45) (a) Küchle, W.; Dolg, M.; Stoll, H.; Preuss, H. Energy-adjusted pseudopotentials for the actinides. Parameter sets and test calculations for thorium and thorium monoxide. *J. Chem. Phys.* **1994**, *100*, 7535−7542. (b) Leininger, T.; Nicklass, A.; Stoll, H.; Dolg, M.; Schwerdtfeger, P. The accuracy of the pseudopotential approximation. II. A comparison of various core sizes for indium pseudopotentials in calculations for spectroscopic constants of InH, InF, and InCl. *J. Chem. Phys.* **1996**, *105*, 1052−1059.
(46) Zhao, Y.; Truhlar, D. G. The M06 suite of density functionals for main group thermochemistry, thermochemical kinetics, noncovalent interactions, excited states, and transition elements: two new functionals and systematic testing of four M06-class functionals and 12 other functionals. *Theor. Chem. Acc.* **2008**, *120*, 215−241.
(47) Weigend, F.; Ahlrichs, R. Balanced basis sets of split valence, triple zeta valence and quadruple zeta valence quality for H to Rn: Design and assessment of accuracy. *Phys. Chem. Chem. Phys.* **2005**, *7*, 3297−3305.
(48) Barone, V.; Cossi, M. Quantum Calculation of Molecular Energies and Energy Gradients in Solution by a Conductor Solvent Model. *J. Phys. Chem. A* **1998**, *102*, 1995−2001.
(49) Tomasi, J.; Persico, M. Molecular Interactions in Solution: An Overview of Methods Based on Continuous Distributions of the Solvent. *Chem. Rev.* **1994**, *94*, 2027−2094.
(50) Schleyer, P. v. R.; Maerker, C.; Dransfeld, A.; Jiao, H.; van Eikema Hommes, N. J. R. Nucleus-Independent Chemical Shifts: A Simple and Efficient Aromaticity Probe. *J. Am. Chem. Soc.* **1996**, *118*, 6317−6318.
(51) Chen, Z.; Wannere, C. S.; Corminboeuf, C.; Puchta, R.; Schleyer, P. v. R. Nucleus-independent chemical shifts (NICS) as an aromaticity criterion. *Chem. Rev.* **2005**, *105*, 3842−3888.
(52) Matito, E. *ESI-3D*; IQCC and DIPC: Donostia Euskadi, Spain, 2015.
(53) Matito, E.; Poater, J.; Duran, M.; Solà, M. An analysis of the changes in aromaticity and planarity along the reaction path of the simplest Diels-Alder reaction. Exploring the validity of different

https://doi.org/10.1021/acs.organomet.2c00099
Organometallics 2022, 41, 1204−1215

indicators of aromaticity. *J. Mol. Struct.: THEOCHEM* **2005**, *727*, 165−171.
(54) Salvador, P.; Ramos-Cordoba, E. An Approximation to Bader's Topological Atom. *J. Chem. Phys.* **2013**, *139*, No. 071103.

https://doi.org/10.1021/acs.organomet.2c00099
Organometallics 2022, 41, 1204−1215